IMAGE PROCESSING SUGGESTIONS FOR ASTRONOMICAL MULTIEXPOSURE WIDE FIELD PLATES [1]

DIMO DIMOV[1] and MILAN S. DIMITRIJEVIĆ[2]

[1]*Inst. of Information and Communication Technologies, BAS, Sofia*
[2]*Astronomical Observatory, Belgrade*
E-mails: dtdim@iinf.bas.bg, mdimitrijevic@aob.bg.ac.rs

Abstract: In the article is proposed how to assess the quality of archival plates with chains. Certainly, CCD astronomy replacing classical photo astronomy recently makes senseless use of multiexposure wide-field plates (MEWFP) approaches. On the other hand, the world heritage of archive MEWFP, with 4-6 expositions estimated at over 10,000, encourages the development of specific methods for computer processing of MEWFP. Thus, our method is useful to evaluate the structural quality of archival MEWFP (whether it is exacerbated by overlapping of star copies on the plates).

1. INTRODUCTION

The method for locating non-stationary (variable and/or quickly moving) stellar objects by capturing images of star chains is known in astronomy as multiexposure method. The method consists of repeated photo exposures (on the same photo plate) of the observed celestial quadrant. Photo exposures, usually 4 to 6 in number, are equal over time (e.g. $\sim 5 \div 10$ min each) and relative (mechanical) movements of the photo plate toward the instrument (telescope) are uniform from exposure to exposure in selected fixed direction. The exception is the first shift, which is ~ 2 times larger than the other to indicate the beginning of the chains (Aniol et a., 1990, Winterberg et al., 1995).

The idea for this report comes from the difficulty of comprehensive computer processing of plates with star chains (Dimov et al., 2012). The configuration of the chains in a plate is usually static, i.e. direction of the chains and the distances

between their components (copies of the star over time) were selected from astronomers mainly on the principle of operational ease of use with the given telescope. Thus, in the inherited, during the years, archive plates we meet too many instances of (partially or completely) overlapping star chains, which hinders comprehensive identification of all chains in the plate for the accurate localization of flare star phenomena looked for.

In comparison to the original MEWFP method, the proposed method seems a little late in time, in view of the incoming CCD technology to replace the classical photography in astronomy. There are no technological limits to playing MEWFP method in CCD technology[2]. But this is proved unnecessary because the sequence of CCD images can directly (and more efficiently) be processed by the so-called image differencing approaches[3] (Sonka, Hlavac and Boyle, 1998).

On the other hand, the world heritage of archival astronomical plates with 4-6 expositions could be estimated at least over 10 000, according to the data in (Tsvetkova, 2012), which stimulates the development of specific methods for computer processing (Aniol et al., 1990, Winterberg et al., 1995, Dimov et al., 2012). Method proposed here can be used to assess the quality of existing archival images with MEWFP chains, in particular − to their structural quality determined by proximity to the optimum structure of the chains (as direction and distance between components). Evaluation is obtained a posteriori, i.e. concerns quality of an (already) conducted MEWFP experiment with star chains. It may serve to substantial improvements in computer processing of MEWFP images, e.g. Dimov et al. (2012), for an (external, independent) evaluation of the error in variable chains demand, i.e. variations caused by variable stars rather than random overlap in MEWFP experiment.

2. PROPOSED METHOD DESCRIPTION

2.1. Preliminary observations

We assume that the input image is pre-processed to an adequately binarized image, i.e. stars are presented by "white" spots against the "black" sky. This type of astro images are considered as "positives", unlike the original negative images obtained by scanning astronomical plates.

For the purposes of this experiment we will use a preview to astronomical image of the Pleiades region, see Fig. 1a, and its corresponding positive − in Fig. 1b.

---

[2] http://en.wikipedia.org/wiki/Charge-coupled_device
[3] http://en.wikipedia.org/wiki/Blink_comparator

(a)

(b)
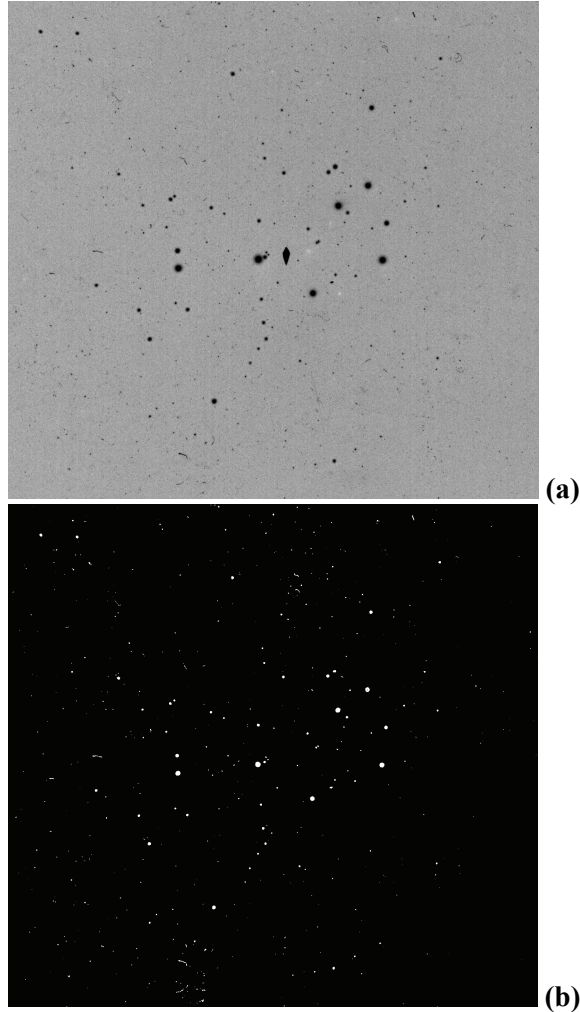
Figure 1: Image cluster "Pleiades": a) an original preview-negative 1682x1580 pix; a (diamond like) artifact is observed in the image center caused by photo plate storage in the time; b) the working positive (after binarization of the original), where the artifact is cleaned interactively.

We will mainly consider the case of linear chains (Aniol et al., 1990, Winterberg et al., 1995, Dimov et al., 2012), see also Fig. 2. Without loss of generality (and for definiteness of illustrations), we will consider the most common case:

$$d_{1,2} = 2d, \quad d_{2,3} = d_{3,4} = d_{4,5} = d_{5,6} = d, \ d > 0, \tag{1}$$

where $d_{i,i+1}$, $i = 1,...,(n-1)$ are the distances between the consecutive chain components and the length n (in number of components) is $n = 6$. Cases of "non-

linear" chains described in Dimov et al. (2012), see Fig. 2b, will be considered in discussions later on.

We substantially use analogies with the concepts, *cumulative image* and *reduced cumulative image*, introduced in [3] for the identification of chains in astro images. Here we interpret these concepts for generating images with chains from a single image of a given sky quadrant.

2.2. Idea of the method

***Step* S1:** Let us choose an arbitrary star in the input working image. Since there black areas indicate the absence of significant stars, we can give the following trivial interpretation – black areas mark the possible vectors of displacement of the plate (to receive any chain with $n = 2$, but only for the selected star), so the shift up of this star (in the new exposure of the plate) does not cover any other star.
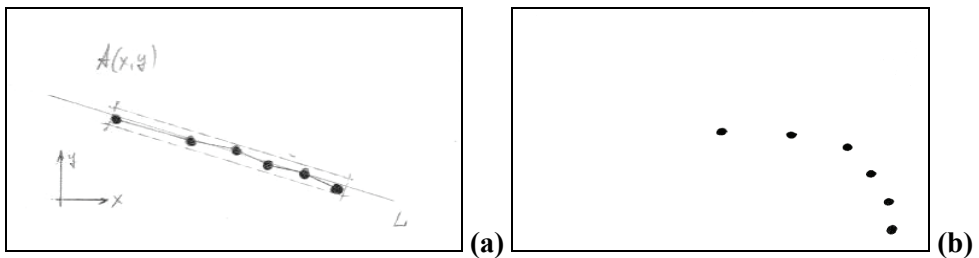
Figure 2: Chain schemes with $n = 6$ components (i.e., n exposures of the plate): a) a linear scheme of chain with illustration of the chain average direction L; b) a non-linear scheme, for details, see [3].

For definiteness, and without loss of generality, we consider that the Cartesian coordinates' origin of the image is moved to the center of the chosen star, i.e. that the star coordinates are (0,0).

***Step* S2:** Let us choose another star with coordinates (x_2, y_2) of its center, get a copy of the input image and impose it upon the previous one, but translated so that the selected second star to coincide with the first one (from step S1). Thus, each pixel (x, y) of the input image is shift τ_2 translated to position $(\widetilde{x}, \widetilde{y})$, and the second star is also provided with coordinates (0,0) after translation:

$$(\widetilde{x}, \widetilde{y}) = (x, y) - \tau_2,$$
$$\tau_2 = (x_2, y_2) - (x_{size}/2, y_{size}/2), \quad 0 \le x < x_{size}, \quad 0 \le y < y_{size} \tag{2}$$

where x_{size} and y_{size} define the size of the input working image in pixels.

Now, if we add disjunctively the both images, primary and shifted ones then the resultant black areas will mark the possible positions of the second component

of any chain of length $n = 2$ (but only for the first star and for the second star), do not cover any other star.

Step S3: Repeat the previous step S2 for all other stars in the image. Then, the black areas in resultant (disjunctive) image will mark the option for vector displacements of the plate (i.e., the formation of all chains with length $n = 2$ components), so that no chain can fall on another chain, and more precisely, any particular chain component does not cover any components of other chains.

For formal completeness, we determine starting with a blank (i.e. entirely black) image whose coordinate system is at its center, i.e. that at the current step S3 we brought all the stars found in the input image in the blank image center, like the first star (at S1) and the second one (at S2). The resultant image will be called *disjunctive accumulated image* (DAI).

DAI has the same properties as the accumulated image that had been already described, although for other purposes in Dimov et al. (2012). By analogy with Dimov et al. (2012), we also restrict a substantial square of size *a*, $a = \min\{x_{\text{size}}, y_{\text{size}}\}/2$, in the central part of DAI, and we call it "*reduced* DAI" (RDI). Obviously, the area outside RDI contains incomplete information about chains overlap, because the area of the original input image, which is also used in the assessment, is uncertain therein and is formally declared by us to empty (all black). An example of DAI is illustrated in Fig. 3, and the respective and only significant RDI – in Fig. 4b. Note that zooming of images in detached figures varies for better illustration, where matching size can be traced by means of squared hints in the figures, see Fig. 3 and Fig. 4.

2.3. Formal description of the method

Step S4: Let us scale the received RDI by a factor 3/2 and limit the result to the initial RDI size towards the coordinate origin. For the resultant, scaled and centered image to mark it as SDI(3), we can write formally:

$$\text{SDI}(3) \Leftarrow \text{RDI}: \left\{ I(\widetilde{x}, \widetilde{y}) = I(x, y), (\widetilde{x}, \widetilde{y}) = \frac{3}{2}(x, y), \ (\widetilde{x}, \widetilde{y}) \in \text{SDI}(3), (x, y) \in \text{RDI} \right\}, \ (3)$$

where $I(\widetilde{x}, \widetilde{y})$ and $I(x, y)$ are the intensity values of the pixels in the SDI(3) and RDI. Let us summarize (disjunctively, pixel by pixel) the two images and indicate the result as RDI(3):

$$\text{RDI}(3) = \text{SCDI}(3) \cup \text{RDI} . \tag{4}$$

It can be shown that the black areas in the resultant image RDI(3) represent a mask for possible displacement of the plate, i.e. for optimal selection of a structure of no overlapping chains with length $n = 3$ components. Indeed, if we choose a point (pixel) in the black area of RDI(3), then it is guaranteed with a corresponding (affine, projective) point in the black area of RDI.

Repeat the previous step iteratively, i.e. scaling (3) and disjunction (4) until the desired length *n* of chains, for example, until *n* = 6.
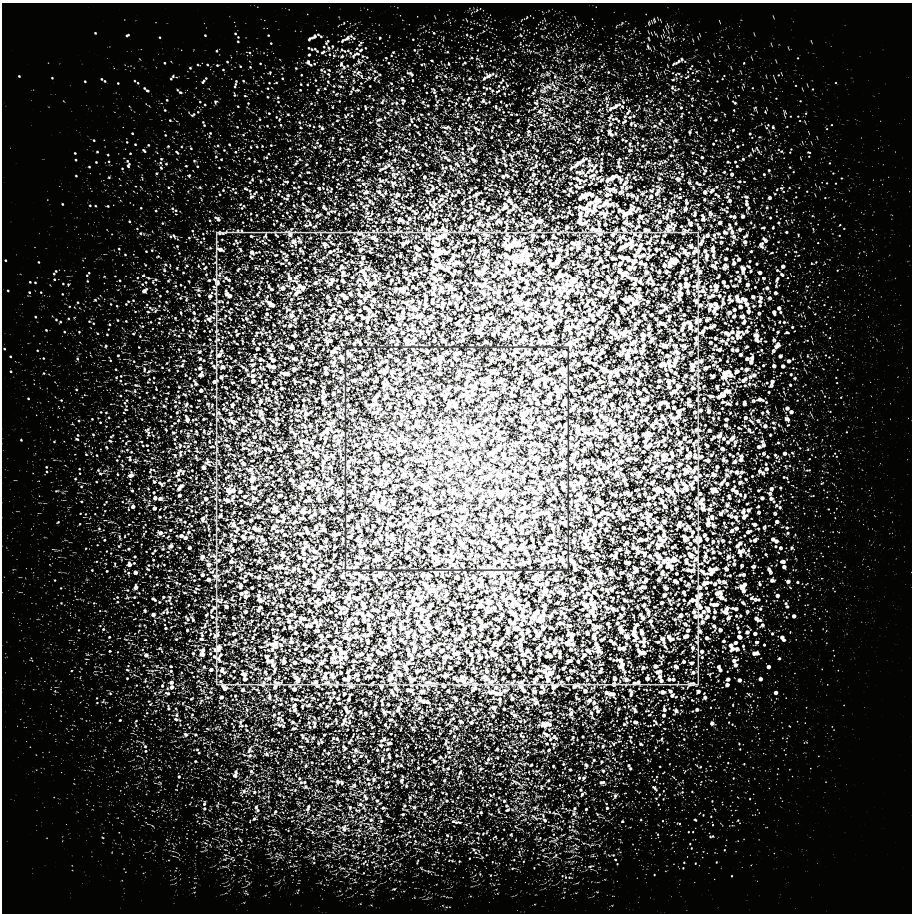
If we formally write for the first step S1:

$$RDI(2) = RDI , \tag{5}$$

then we can summarize the description (3) and (4) by the following recursive formulae:

$$RDI(i) = SDI(i) \cup RDI(i-1), \; i = 3, \ldots, n; \tag{5a}$$

where

$$SDI(i) \Leftarrow RDI(i-1) : \left\{ I(\widetilde{x}, \widetilde{y}) = I(x, y), (\widetilde{x}, \widetilde{y}) = \frac{i}{i-1}(x, y), \; (\widetilde{x}, \widetilde{y}) \in SDI(i), (x, y) \in RDI(i-1) \right\} \tag{5b}$$

Figure 3: Full accumulated disjunctive image DAI, derived from the binarized input image (Fig. 1b). The position and size of both, the input image and the reduced disjunctive image RDI, are pointed by extra square hints.

The final image RDI(n) of the sequence RDI(i), $i = 2, \ldots, n$, shows the optimal choice of the last, n-th component of the chains of the desired length of n components. Indeed, if we choose a point in the black area of RDI(6), it follows that it is guaranteed with a series of corresponding (affine) points from black areas of each one of the images RDI(5), RDI(4), RDI(3) and RDI(2), and that these points can be used to structure the chains of type (1), which first component is the beginning (0,0), i.e. the common center of these RDI images.

Now, we can specify the intuitively used concept of "*optimal choice of linear chains structure*" by the following:

Statement: Each chain structure choice by the above method is optimal in the sense that the centers of all the components of the chains generated for the stars found in the input image will fall only in the free (black) areas and not on other components and/or stars. Something else, if the mask RDI(i) be empty for some i, $2 \leq i \leq n$, then the task of optimal chains with the number of components $\geq i$, has no solution.

Proof: ♦ Since working images here are black and white only, we can consider white areas (i.e., star spots) as sets of logical (Boolean) units, and black areas as sets logical (Boolean) zeros. Thus, for a set A of image pixels, we will denote by $\overline{A}$, $\overline{A} \subset A$, the subset of black pixels only.

Let us choose a point C_n (a vector $\overrightarrow{C_n}$) from the black field of RDI(n), i.e.,
$$C_n \in \overline{\mathrm{RDI}(n)} \neq \varnothing.$$

Then from definition (5a,b) applied to RDI(n):
$$\mathrm{RDI}(n) = \left(\frac{n}{n-1} * \mathrm{RDI}(n-1) \right) \cup \mathrm{RDI}(n-1),$$ and from de Morgan's laws for the Boolean intensities of each pixel, it follows that $C_n \in \left(\frac{n}{n-1} * \overline{\mathrm{RDI}(n-1)} \right) \cap$

$C_n \in \overline{\mathrm{RDI}(n-1)}$, where the two-place operation $a*A$ denotes scaling a given point (vector) set A by a coefficient a towards the initial point (vector) C_0, $\left| \overrightarrow{C_0} \right| \equiv 0$. Consequently: $\exists! C_{n-1}$, $C_{n-1} \in \overline{\mathrm{RDI}(n-1)}$, where $\overrightarrow{C_{n-1}} = \left(\frac{n-1}{n} \right) \overrightarrow{C_n}$, for the chosen $C_n \in \overline{\mathrm{RDI}(n)}$.

In this way, recursively it follows that for each point $C_i \in \overline{\mathrm{RDI}(i)}$, $i = n, \ldots, 3$, it exists an unique point $C_{i-1} \in \overline{\mathrm{RDI}(i-1)}$ such that $\overrightarrow{C_{i-1}} = \frac{i-1}{i} \overrightarrow{C_i}$. Hence, the vectors $\overrightarrow{C_i}$, $i = 2, \ldots, n$, are collinear, and the points C_i, $i = 1, \ldots, n$ are situated on an unique line.

Finally, for the $\overrightarrow{C_2}$ component of the chains, we have $C_2 \in \overline{\text{RDI}(2)}$, wherefrom according to (5) it follows that $\left|\overrightarrow{C_1}\right| \equiv 0$, which ends the proof. ♦

Fig. 4(b÷f) show the masks RDI(i) for optimal selection of the plate displacement, for each length i of the chains, respectively $i = 2,3,4,5,6$. Fig. 4a refers to the formal chain of length i=1 component, i.e. it coincides with the input binarized image (cf. Fig. 1b).

2.4. Enhanced interpretation of the method

In such a way, each pixel in the black area of RDI(6), if non-empty, is a solution to our task.

• In case one gives some requirements for physical dimensions of the chains, as in celestial degrees (or minutes, or seconds) or in pixels, then we can sort pixels of free (black) areas according to their distances to the RDI center and look for an optimum on this sorting.

• Since stars on astro images are not ideal (mathematical) points but real spots (of significant intensity measurement), see Fig. 1(a,b), it is actually a good idea in the free (black) areas to look not as for isolated pixels but for circular areas with a diameter of more than average amount over all stellar spots in the image. For example, in the present working image of the Pleiades (Fig. 2b) the average diameter of the star spots is ~3.9 pixels, while the maximum diameter is ~17.3 pixels.

• So far, we discussed the simplest (and most used) chain structure − linear structure, in which the distances between the components of the chains are given by (1) (see also Aniol et al., 1990, Winterberg et al., 1995).
Obviously, for generality of results, we may consider arbitrary structure of chains such as Fig. 2b, i.e. when, instead of (1), we ask an arbitrary chain structure through respective vector displacements of components towards the starting component (the original star) (Dimov et al., 2012):

$$\overrightarrow{C_i} = (x_i, y_i) - (x_1, y_1), \; i = 1,...,n, \tag{6}$$

where (x_i, y_i) are the vectors (i.e. centers) of components of a given chain towards the beginning (first component) $\overrightarrow{C_1} = (0,0)$ of the chain. Furthermore to this general case, it is sufficient to add rotation of SDI(i) at angle φ_i at step S4, after scaling (5b), as follows:

$$\text{rSDI}(i) \Leftarrow \text{SDI}(i) : \left\{ I(\tilde{x}, \tilde{y}) = I(x, y), \ (\tilde{x}, \tilde{y}) = (x, y) \left\| \begin{matrix} \cos\varphi_i & -\sin\varphi_i \\ \sin\varphi_i & \cos\varphi_i \end{matrix} \right\|, \ (\tilde{x}, \tilde{y}) \in \text{rSDI}(i), (x, y) \in \text{SDI}(i) \right\}$$

$$\text{SDI}(i) := \text{rSDI}(i) \ ,$$

(6a)

where $\varphi_i = \angle(C_{i-1}, C_i)$, $i = 3,...,n$, see also Fig. 2b, where n=6.

By the way, the linear case (1) can be represented by (6) and (6a), like:

$$d_{1,2} = \left| \overrightarrow{C_1} - \overrightarrow{C_2} \right| = 2d \ , \quad d_{i,i+1} = \left| \overrightarrow{C_i} - \overrightarrow{C_{i+1}} \right| = d, \quad i = 2,...,(n-1), \qquad (7)$$

and $\varphi_i \equiv 0, \ i = 3,...,n$, n=6.

2.5. The Algorithm Proposed

Input data:

- Astro image (a negative, an original or preview) N, $0 \le N(x, y) < L_{\max}$, $(x, y) \in [x_{\text{size}} \times y_{\text{size}}]$, where $[x_{\text{size}} \times y_{\text{size}}]$ is the domain of N, x_{size} and y_{size} are in pixels, and $L_{\max} - 1$ is the possible maximum of image intensity values ($L_{\max}$ is natural number usually written in the image file format).
- Number n of the components of wanted chains, usually $3 \le n \le 6$.

NB.: For overall processing speed use as simple preview as possible, while the stars of interest (or of given magnitude) are still visible on the preview. Over this limit, the preview precision used does not affect essentially the method performance.

Expected result:

♦ Slope α (in radians) of the chain direction towards the abscissa in the image N, and

♦ Basic distance d for the components, according to (1) or (7).

We describe the algorithm in two main steps: pre (A1) and core (A2):

A1) *Preprocessing:* Evaluation of the centroides (mass centers of the star spots) in the image. For this purpose:

♠ Invert the input image (see Fig. 1) from negative N to positive P by the formulae:

$$\forall (x, y)\big((x, y) \in [x_{\text{size}} \times y_{\text{size}}]\big): \ P(x, y) = L_{\max} - N(x, y) - 1, \qquad (8)$$

where $[x_{\text{size}} \times y_{\text{size}}]$ is the domain either for N or for P.

♠ Binarize the received positive P to get input working image B (see Fig. 1b), by the formulae:

$$\forall (x,y)(0 \le x < x_{\text{size}}, 0 \le y < y_{\text{size}}): \quad B(x,y) = \begin{cases} L_{\max} - 1, & \text{if } P(x,y) < t(x,y) \\ 0, & \text{if } P(x,y) \ge t(x,y) \end{cases}, \quad (9)$$

where $t(x,y)(0 \le x < x_{\text{size}}, 0 \le y < y_{\text{size}})$ is binarizing (threshold) surface in the general case of locally adaptive binarization, see for example (Dimov and Dimov, 2010). In relatively "clean" images: $t(x,y) = t_0 = \text{cte}$, t_0 a threshold for global binarization, $0 \le t_0 < L_{\max}$.

♠ Find the center of mass (centroide) of each star spot. In our case, for simplicity of demonstrations, we work directly with binarized image *B*. For larger precision, binarized image *B* can be used as a mask for positive input *P* in assessing the centroides.

NB.: Finding centroides can be also conducted through sophisticated computer software for registration of astronomical images, e.g., the program SExtractor (Bertin and Arnouts, 1996), and then computer to generate the working image *B* using stars data (declination, right ascension and magnitude) registered in the corresponding to B area of used sky catalog. This approach, however, is very resource intensive and unnecessarily precise for the intended purpose here.

A2) *Basic processing:* As described in paragraph 2.2 and 2.3:

♥ Generate initial RDI, pursuant to paragraph 2.2 (see also Fig. 4b). Announce RDI(2) = RDI.

♥ Generate cyclically all RDI(*i*), *i* = 3,…*n*, according to (5a) and (5b) in paragraph 2.3.

♥ Look for position of the optimal chain in the black areas of the RDI(*n*), i.e. in $\overline{\text{RDI}(n)}$.

Here, various heuristics are possible, such as:

- Find the solution $(x_{\text{opti}}, y_{\text{opti}})$, $(x_{\text{opti}}, y_{\text{opti}}) \in \overline{\text{RDI}(n)}$, as the minimum $D_{\min}$ of distances $D = \sqrt{x^2 + y^2}$ from all points $(x,y) \in \overline{\text{RDI}(n)}$ to the image center, either

- The same, but with the following premise: look for $(x_{\text{opti}}, y_{\text{opti}})$, not as an isolated pixel, but as the center of isolated circle of diameter ϕ, $\phi > 0$. An upper limit for ϕ can be determined at step A1, for example, as the average (or maximal) diameter of star spots in the working image *B*;

- Other heuristics.

♥ Calculate the expected result:

$$\alpha = \text{tg}(y_{\text{opti}} / x_{\text{opti}}), \quad d = \sqrt{x_{\text{opti}}^2 + y_{\text{opti}}^2} \Big/ n \qquad (10)$$

End of algorithm.

NB.: The existence of a solution for working binarized image B, i.e. $\exists \big((x,y) \in \mathrm{RDI}(n) \big) \big(I(x,y) = 0 \big)$ or what is the same: $\left| \overline{\mathrm{RDI}(n)} \right| > 0$, obviously leads to the existence of a solution for the original image N too.

3. EXPERIMENTS AND DISCUSSION

3.1. Experiments

A standard Windows-7/Vista/XP application is performed to test the proposed method for the estimation how good was the choice of the plate movements. The application is C/C++ written in a Borland C Builder 5.0 environment. The experimental computer is an IBM compatible PC: Intel Core 2 Quad CPU 2.8 GHz, MM 4,0 GB. The input images should be preliminary converted to Windows BMP/JPG format (1 bpp).

A preview image of the Pleiades region has been used for experiments, whose dimensions are $(x_{\mathrm{size}}, y_{\mathrm{size}}) = (1682, 1580)$, see also Fig. 1. The length n of the chains is chosen: $n = 6$.

The result of the proposed algorithm performance on the image (cf. Fig. 4f) is as follows: $(x_{\mathrm{opti}}, y_{\mathrm{opti}}) = (331, 372)$, where the RDI(6) domain is a square of size 780.

Consequently $(\widetilde{x}_{\mathrm{opti}}, \widetilde{y}_{\mathrm{opti}}) = (\text{-}59, \text{-}18)$, according to (2), wherefrom to (10), we have:
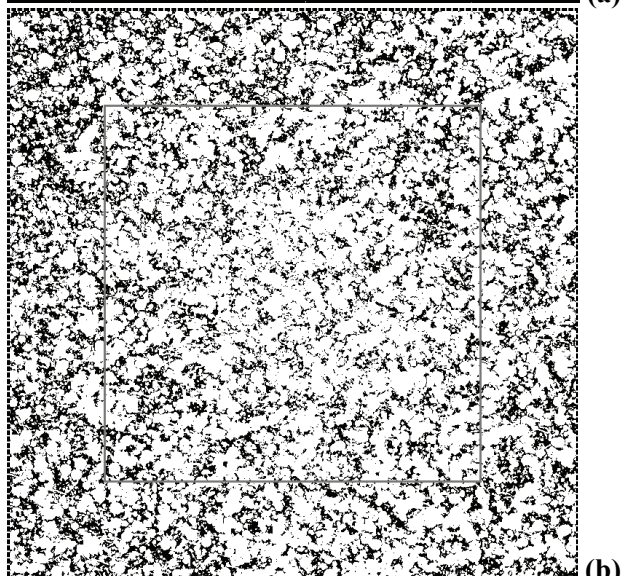
$$D_{\min} = 61.2 , \; d = 10.2 , \; \alpha = -163.0° , \tag{11}$$

hence for the optimal structure of the chains (in central coordinates, and restrictively to pixel precision) we obtain:
$(0,0), (\text{-}20, \text{-}6), (\text{-}29, \text{-}9), (\text{-}39, \text{-}12), (\text{-}49, \text{-}15), (\text{-}59, \text{-}18)$.
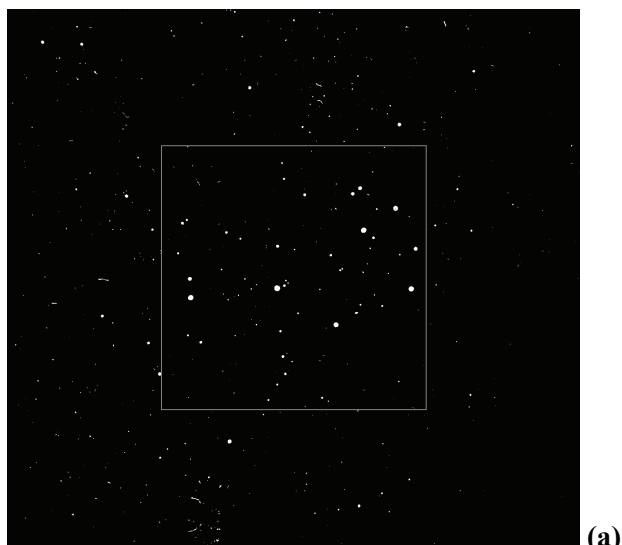
(a)

(b)

(c)

(d)

(e)

(f)
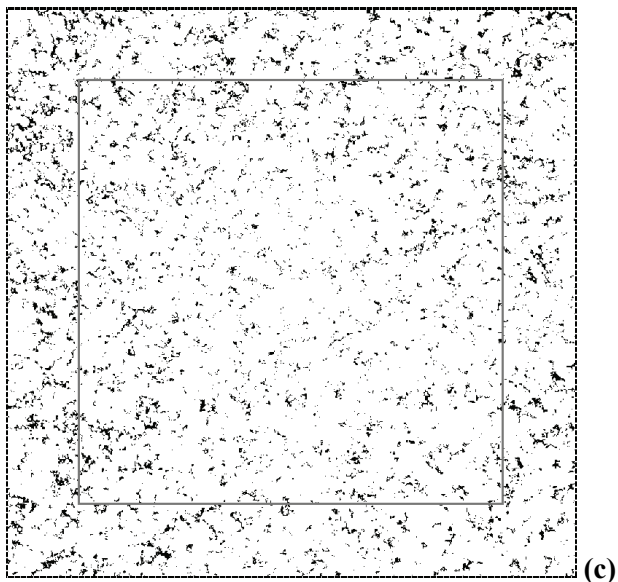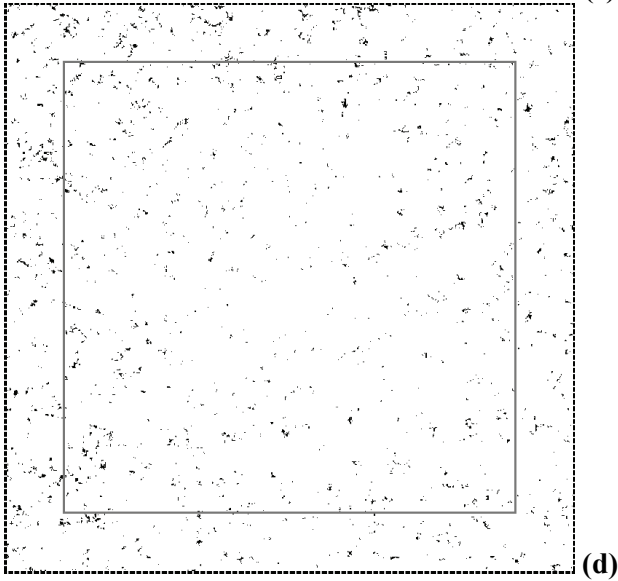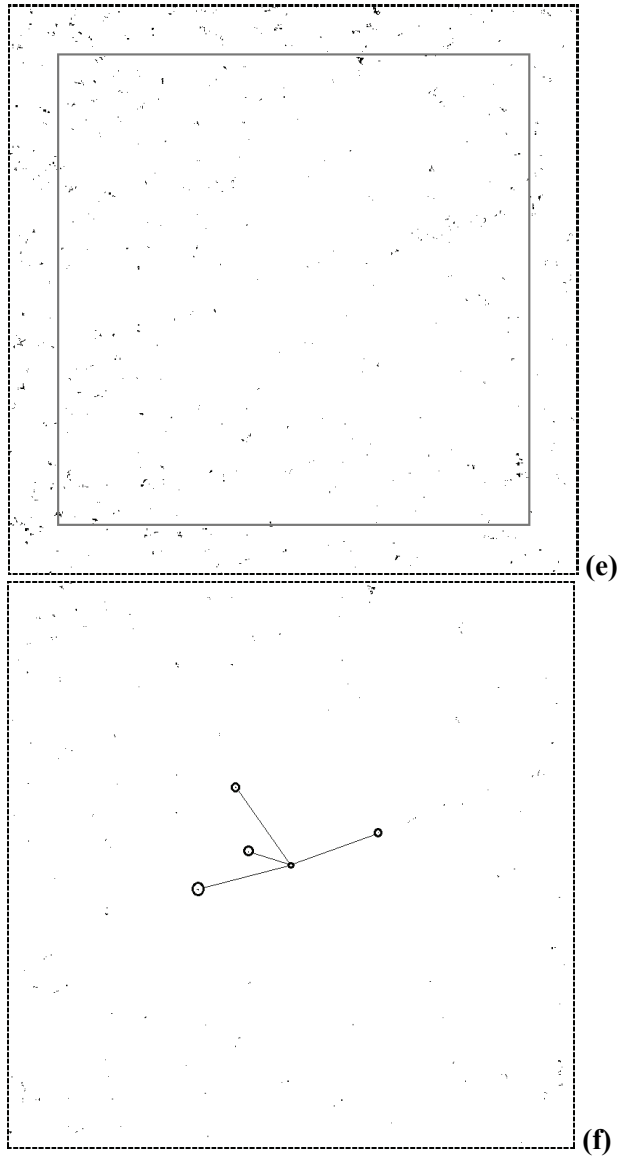
Figure 4: A sequence of reduced accumulated images RDI (*n*): a) *n* = 1 (formally), b) *n* = 2 (RDI), c) *n*=3, d) *n*=4, e) *n*=5, and f) *n*=6. Black areas of each RDI mark the current (*n*-th) component for selecting non-overlapping chains. Also, the position and size of next RDI is graphically illustrated by respective artifact-rectangle herein.

The sequence of reduced accumulated images, RDI(*i*), *i* = 1, ... 6, associated with the proposed method and algorithm, is illustrated in Fig. 4(a÷f). Black areas in RDI(*i*), i.e. relevant $\overline{\text{RDI}(i)}$, mark the position of *i*-th component for selecting

of non-overlapping chains. An artificial square hint on each RDI(i) marks the position and size of the next RDI($i+1$), $i=1,\ldots5$, for better understanding of illustrations. For similar reasons, the sequence beginning is prefaced by the work image B (see also Fig. 1b), which plays a formal role as RDI(1). On RDI(6), i.e. last RDI, the first few (closest to the center) opportunities for chains' choice are illustrated, including the above announced optimal solution. The corresponding precise values of these solutions are given in Table 1.

Table 1: Choice of (linear) chains parameters for the image of Fig. 1a.

No.	(x_{opti}, y_{opti})	$(\widetilde{x}_{opti}, \widetilde{y}_{opti})$	D_{min}	d [pix]	α [degrees]	$\varnothing$ [pix]	Overlaps %
1	(331, 372)	(-59, -18)	61.7	10.3	-163.0	1.5	4.9
2	(510, 345)	(120, -45)	128.2	21.4	-20.6	1.0	-
3	(313, 282)	(-77, -108)	132.6	22.1	-125.5	2.5	-
4	(261, 423)	(-129, 33)	133.2	22.2	165.7	2.5	-
*	(413, 388)	(23, -2)	24.0	4.0	-3.2	-	29.0

Each row of Table 1 corresponds to possible choice of the (linear) chains parameters for the image B, i.e., for the input image N too. The table rows are sorted in ascending order of D_{min}. Thus, row 1 represents the optimal choice for chains parameters, and the corresponding image of chains artificially generated for this choice is illustrated in Fig. 5a. The last column of the Table assesses the overlap area among the chains as a percentage of the maximum possible area A_{ovr} of overlap, $A_{ovr} = (n-1)S$, $n = 6$, and S the total area of stellar spots localized in the input image.

It is clear from Table 1 that if seeking a minimum length of the chains, and the diameter of the circle of guaranteed non-overlapping is, for example, $\phi = 2$, then instead of the obvious choice (row 1), we should prefer row 3 of the Table.

(a)

(b)
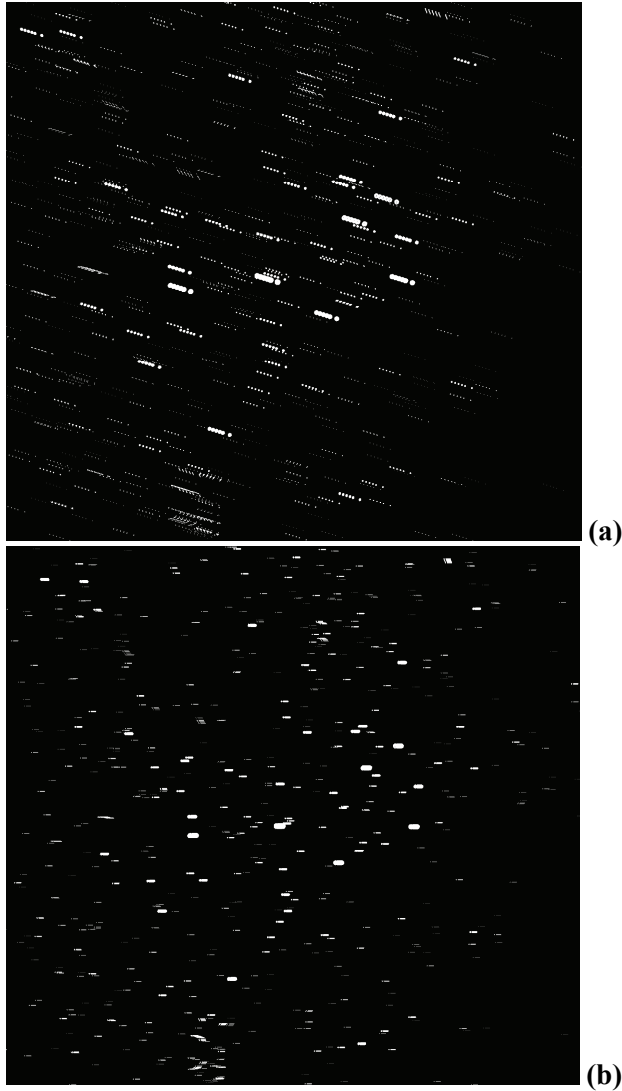
Figure 5: Astro image with chains (of 6 components' length): a) the optimal astro image (with a slope of chains α = 163.0°, d = 61 [pix]), generated from the working image of Fig. 1b; and b) generated (from Fig. 1b) a virtual copy of the original image ROZ050_000046 with chains' parameters: α = -3.2°, d = 24.

The last row marked with (*) in Table 1 refers to an image (see Fig. 5b) generated toward the choice that was (ever) made for an archival "Pleiades' chains" image, reviewed in (Dimov et al., 2012). The quantitative evaluation (29%) of overlap here is about 5 times larger than the estimated overlap for the optimal choice (row 1 of Table 1), which can be traced also by visual comparison of Fig. 5(a,b).

3.2. Discussion

The experiment illustrated in Fig. 5, shows the optimal choice of chains (α = 163.0°, d=61 [pix]) following the method proposed here (Fig. 5a), compared to a random choice (Fig. 5b), which parameters α = -3.2° and d=24, are evaluated for the original "Pleiades chains" image, namely ROZ050_000046.bmp (Dimov et al., 2012). Both images (Fig. 5a and Fig. 5b) were obtained through the binarized input image B (Fig. 1b) by generating the appropriate software chains to simulate as close as possible experimental conditions in the two cases under comparison.

In fact, the differences in the both experiments are essential − the first one is incomplete (no actual image of chains were produced, we have only the input image of Fig. 1), while the second is represented only by an image with chains, and no initial image (like in Fig. 1). We should consider differences in experiment dates, hence varying degrees of aging of the plates, as well as differences in the type of plates, duration of exposure, type of telescopes used, etc.

Further, and beyond the illustrated comparison, we can see that the chains' overlap in the original image "Pleiades' chains" of Dimov et al. (2012), even above the optimum here defined is not as big as this occurs in its recovery (Fig. 5b) from the input image (Fig. 1). Taking note that the average diameter of the star spots in the input image is about two times larger than the one in the original image with chains from Dimov et al. (2012), explains this discrepancy.

The complexity of the proposed algorithm can be considered linear over the volume of the input image. The measured duration of the experiment is ~1.04 [sec], for the test image volume V = 2.6MB, in a BMP format. So, at the main step A1 of the algorithm proposed, we evaluate an experimental time constant τ, $\tau \sim$ 0.4 [sec/MB], which can be applied to estimate the processing time t for an arbitrary input image, $t \approx V\tau$ [sec].

Interest is the ability to manage the situation of "no solution" at some step i of the proposed algorithm, i.e. when reaching $\overline{|\text{RDI}(i)|} = 0$, $i \le n$. This will summarize two approaches: 1) by manipulating the size of the stellar spots in primary image $B \equiv \text{RDI}(1)$, and 2) by redefining the proposed method − from black-and-white (B/W) images to gray (halftone) ones.

1) If reducing the star spots' diameters ϕ in the image $B \equiv \text{RDI}(1)$ (see Fig. 4a), for example, by a specific operation such as "morphologic erosion" (Sonka, Hlavac and Boyle, 1998) but remaining unchanged the smallest spots, such as $\phi \le$ 2, then the resultant RDI(6) (see Fig. 4f) will obviously contain larger black areas, i.e. more opportunities for optimal selection of chains. Conversely, if an operation like "morphologic dilation" (Sonka, Hlavac and Boyle, 1998), increases the diameter of the spots, even these few options for optimal choice (see also Table 1) will disappear from RDI(6), i.e. problem will become unsolvable at n = 6. We already commented this effect in Fig. 5(a,b), where the differences in the

diameters of stellar spots are due to differences (most likely in duration of exposure at) in both experiment compared.

2) The proposed method was justified here for B/W images. Thus, if at the current step i of the algorithm, the black areas of RDI(i), $i \leq n$, we can choose a circle ϕ, $\phi > \phi_{max}$, where ϕ_{max} is the diameter of the largest star spot in the initial image B, then the method ensures complete lack of overlap between the chains. This is a very strong condition. To avoid early reaching of "no decision" the key condition is weakened to $\phi > \phi_{avrg}$, where ϕ_{avrg} is the average diameter of the star spots in B. We still weaken to $\phi > 0$, which allows for larger values of n, at the expense of minor overlaps on the periphery of the chains. This brings the idea of an extension defined on the halftone images instead of B/W ones. To do this:

- Define a new initial image B_E, $B_E = B \cap P$, P the original input image, and B is its binarization used as mask to pass only essential (above the binarization threshold) intensities of star spots in P;

- Instead of disjunction in (4) and (5a) use an "extended disjunction", i.e. like the conventional summation but restricted above by the intensity L_{max}, $L_{max}=256$ for P and B_E images, $B_E \equiv$ RDI$_E$(1), as well as for the subsequent RDI$_E$(i) and SDI$_E$(i), $i=2,\ldots,n$;

- Look for the optimal solution (x_{opti}, y_{opti}) like a point (pixel) in RDI$_E$(n), where the intensity of RDI$_E$(n) reaches (a local) minimum.

Fig. 6(a,b) illustrates the comparison of final results obtained by the basic B/W method and by its halftone extension both applied to the same example, cf. Fig. 4f.

(a)

(b)
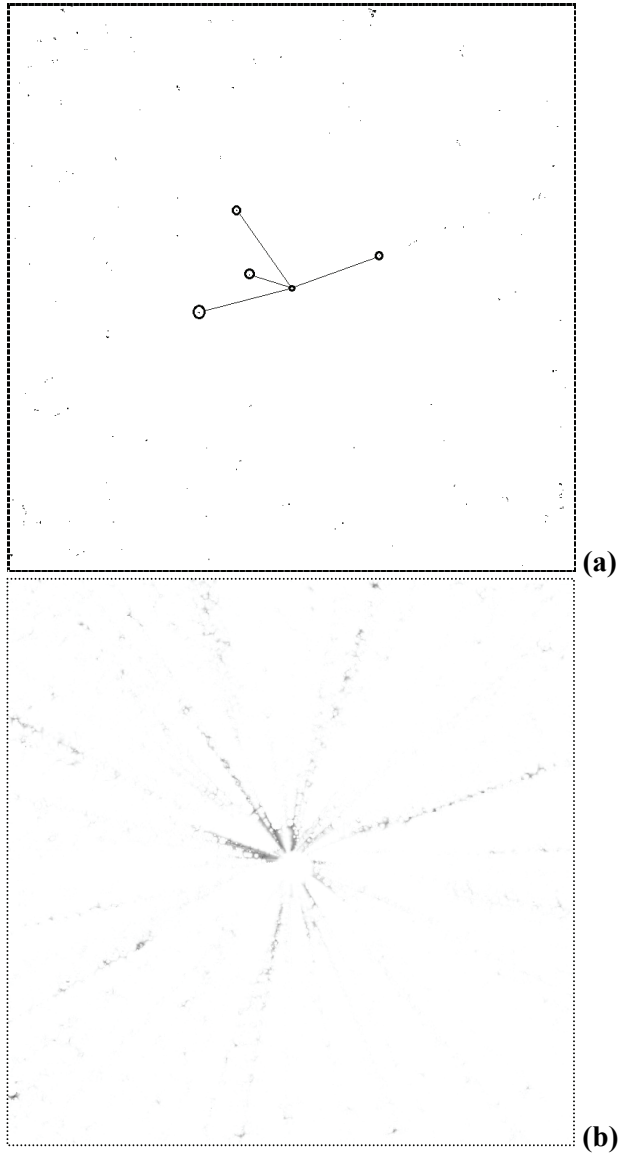
Figure 6: Comparison between of the proposed B/W method and its halftone extension: a) resultant B/W RDI(6) copied from Fig. 4f; and b) corresponding halftone result $RDI_E(6)$. Obviously, the ability to define an optimal choice for the halftone expansion is significantly more flexible.

4. CONCLUSION

The method presented here, algorithm and program are developed for evaluation of optimal design parameters (slope and reference distances) of the chains in the astronomical MEWFP method.

The proposed method is described for linear chains structure and is generalized for synthesis of arbitrary (non-linear) chains structure. Various modifications of the basic B/W method are discussed including its halftone expansion, leading to an optimal compromise in no-decision cases by the basic method.

The primary purpose of this development is for a posteriori evaluation of the structural quality of (images of) astronomical archives of MEWFP type. Evaluating whether (and how much) the quality is exacerbated by overlapping stellar copies, allows improvements in demand for really variable stellar objects in archival (available, known) MEWFP. And this is considered important because of the large number of known and/or available MEWFP in astronomical observatories archives around the world.

References

Aniol, R., Duerbeck, H. W., Seitter, W. C., Tsvetkov, M. K.: 1990, "An automatic search for flare stars in southern stellar aggregates of different ages", In Flare Stars in Star Clusters, Associations and Solar Vicinity, eds. L.V. Mirzoyan, B.R. Pettersen and M.K. Tsvetkov, IAU Symp. 137, Kluwer Acad. Publish., Dordrecht-Boston-London, 85-94.

Bertin, E., Arnouts, S.: 1996, "SExtractor: Software for source extraction", *Astron. Astrophys. Suppl. Series*, **117**, 393-404.

Dimov, D., Dimov, A.: 2010, "Data Driven Approach to Binarization of Astronomical Images", In: Proceedings of CompSysTech'10, June 17-18, 2010, Sofia, Bulgaria, Mini-Symposium on Astroinformatics, ACM International Conf. Proceeding Series, **471**, ACM PRESS, New York, 478-484.

Dimov, D., Tsvetkova, K., Tsvetkov, M., Kolev, A., Kounchev, O.: 2012, "Hough Transform Approach to Flare Stars Identification in Multi-Exposure Plates Images', *Serdica J. Computing*, **6**, 121–148.

Sonka M., Hlavac, V., Boyle, R.: 1998, Image Processing, Analysis, and Machine Vision, 2-d edition, Brooks/Cole Publishing Co., CA.

Tsvetkova, K. P.: 2012, "Astroinformatics for the flare stars in stellar clusters and associations", Proceedings of the VII Bulgarian-Serbian Astronomical Conference (VII BSAC), Chepelare, Bulgaria, June 1-4, 2010, Eds. M. K. Tsvetkov, M. S. Dimitrijević, K. Tsvetkova, O. Kounchev, Ž. Mijajlović, Publ. Astron. Soc. "Rudjer Bošković", **11**, 127-139.

Winterberg, J., Nolte, M., Seitter, W. C., Duerbeck, H. W., Tsvetkov, M. K., Tsvetkova, K. P.: 1995, "Flares and Flashes", Proc. IAU Coll. 151, eds. J. Greiner, H.W. Duerbeck and R.E. Gershberg, Springer Verlag, Berlin, 119.